

Singular point characterization in microscopic flows

Giorgio Volpe,¹ Giovanni Volpe,¹ and Dmitri Petrov^{1,2}

¹*ICFO - Institut de Ciències Fòniques, Mediterranean Technology Park, 08860, Castelldefels (Barcelona), Spain*

²*ICREA - Institució Catalana de Recerca i Estudis Avançats, 08010, Barcelona, Spain*

(Dated: November 2, 2018)

We suggest an approach to microrheology based on optical traps in order to measure fluid fluxes around singular points of fluid flows. We experimentally demonstrate this technique, applying it to the characterization of controlled flows produced by a set of birefringent spheres spinning due to the transfer of light angular momentum. Unlike the previous techniques, this method is able to distinguish between a singular point in a complex flow and the absence of flow at all; furthermore it permits us to characterize the stability of the singular point.

PACS numbers: 47.61.-k, 47.60.+i, 87.80.Cc, 05.40.Jc

Keywords: Microfluidics, Brownian motion, Photonic Force Microscope, Singular points, Stability analysis

The experimental characterization of fluid flows in micro-environments is important both from a fundamental point of view and from an applied one, since for many applications it is required to assess the performance of microfluidic structures, such as lab-on-a-chip devices [1]. Carrying out this kind of measurements can be extremely challenging. In particular, due to the small size of these environments, wall effects can not be neglected [2]. Additional difficulties arise studying biological fluids because of their complex rheological properties.

In the cases of practical interest the flow is strongly viscous (creeping motions or Stokes flows) and a low Reynolds number regime can be assumed [3]. Since the creeping motion regime is a particular case of a laminar regime, it is possible to univocally define a time-independent pressure and velocity field. Therefore, for each position a well-defined drag force acts on a particle immersed in the fluid flow. Ideally micro-flow sensors should be able to monitor the streamlines in real time and in the least invasive way. One common method to achieve this goal is to measure the drag force field acting on a probe particle, resorting to statistical criteria of analysis because of the intrinsic presence of Brownian motion.

Recently optically trapped microscopic particles have been proposed as flow sensors [4, 5, 6, 7, 8]. An optical trap enables the confinement of micron sized objects: a high numerical aperture objective lens is used to tightly focus an optical beam and to produce a force sufficient to hold dielectric objects ranging in size from 100s of nanometers to 10s of microns [9]. In [4] an oscillating optically trapped probe is used to map the two-dimensional flow past a microscopic wedge. In [5] and [6] a stress microrheometer is presented: it generates and measures microscopic fluid velocity fields, monitoring the probe particle displacement, which is directly converted into velocity field values, through digital video microscopy. A further improvement was achieved in [8] by using multiple holographic optical traps in order to parallelize the technique: an array of micro-probes can be simultane-

ously trapped and used to map out the streamlines in a microfluidic device. All these techniques apply a Photonic Force Microscope (PFM) approach [10, 11, 12, 13] to the flow measurement: the fluid velocity at the trap location is obtained by monitoring the probe displacements resulting from the balance between the trapping and drag forces.

All the techniques described above present a major drawback: they interpret the experimental results assuming that the flow can be described by a set of parallel streamlines. When this is the case, the drag force acting on a probe around a specific point in the flow is well described by a constant value, and this is the case considered by the current optical trap methods. However, in the drag force-field there may be singular points as well. In these points the flow and, hence, the drag force are null, but not in its surrounding. The question, which arises naturally, is how to characterize this case. Under the assumption of a steady incompressible flow, a zero body force and low Reynolds numbers, the local fluid motion satisfies the quasi-static Stokes equations [3]: $\eta \nabla^2 \mathbf{v} = \nabla p$, $\nabla \cdot \mathbf{v} = 0$, where \mathbf{v} is the velocity, p is the pressure and η the dynamic viscosity. Since the fluid is incompressible and there are no sources or sinks, there can be only two kinds of singular points [14]: (1) saddles (unstable) at the meeting point between two opposite flowing streamlines or (2) centra (stable) in presence of a non-zero curl. As we show below, the characterization of the flow near these points can be achieved by studying the statistical properties of the Brownian motion of the probe.

The knowledge of the flow-field near a singular point is of relevance for fundamental physical studies as well as for engineering applications. The mixing of fluids flowing through microchannels is important for many chemical application; a reduction of the mixing length can be achieved by the generation of a transverse flow [15], case in which the formation of singular points is inevitable. In biological systems creeping motions take place in small blood or lymphatic vessel or at the interface between tissues and prosthesis or artificial organs [16]. In the presence

of slow flows, macrophage adhesion becomes more probable, increasing the possibilities of inflammation. Furthermore, the growth rate of thrombi, due to platelet aggregation, is also determined by the characteristics of the flow around it: for example, the presence of stable equilibrium points, such as centra, helps their formation and growth [17]. Flow measurements at the microscale can help to diagnose pathologies and to guide the design of bio-materials and nano-devices for diagnostic or therapeutic goals.

In this letter we extend the PFM-approach to microrheology in order to measure and characterize fluid fluxes in the proximity of singular points. The concept is to monitor the position of an optically trapped probe in order to locally characterize the drag force field as a generic function of the space coordinates up to the first order in its Taylor expansion around the probe position [18]. This technique permits us to distinguish between a singular point in a complex flow and the absence of flow at all. Furthermore our approach allows one to determine the stability of these singular points, which can be relevant for applications.

In the following we will consider the drag force field produced by a bidimensional laminar regime. Since in microfluidic and lab-on-a-chip devices a planar geometry is generally assumed, this is the most useful case for applications. Nevertheless, if needed, our approach can be generalized to the three-dimensional case.

Experimentally, we generated these three kinds of fluid flow - namely a set of parallel streamlines, a saddle or a centrum - using solid spheres made of a birefringent material (Calcium Vaterite Crystals (CVC) spheres, radius $R = 1.5 \pm 0.2 \mu\text{m}$ [5]), which can be made spin due to the transfer of orbital angular momentum of light. They are all-optically controlled, i.e. their position can be controlled by an optical trap and their spinning state can be controlled through the polarization state of the light. The angular velocity of the CVC sphere is given by $\omega = \Delta\sigma\lambda P/16\pi^2\eta R^3c$, where $\Delta\sigma$ is the change of the light spin momentum due to the scattering on the probe, P is the beam power, η is the medium viscosity, c is the speed of light, and λ is the wavelength of the optical field. In the experimental realization up to four CVC spheres were optically trapped in water and put into rotation using four steerable 1064 nm beams from a Nd:YAG laser with controllable polarization - to control the direction of the rotation - and power - to control the rotation rate. A probe polystyrene sphere (radius $r = 500 \text{ nm}$) was held by an optical trap produced by a 632 nm linearly polarized beam. The stiffness of this trap was adjustable through the power. The forward scattered light of this latter beam served to track the probe position using a position sensor based on a quadrant-photodetector (QPD).

Assuming no slip at the particle surface, the quasi-Stokes equation leads to the following solution for the

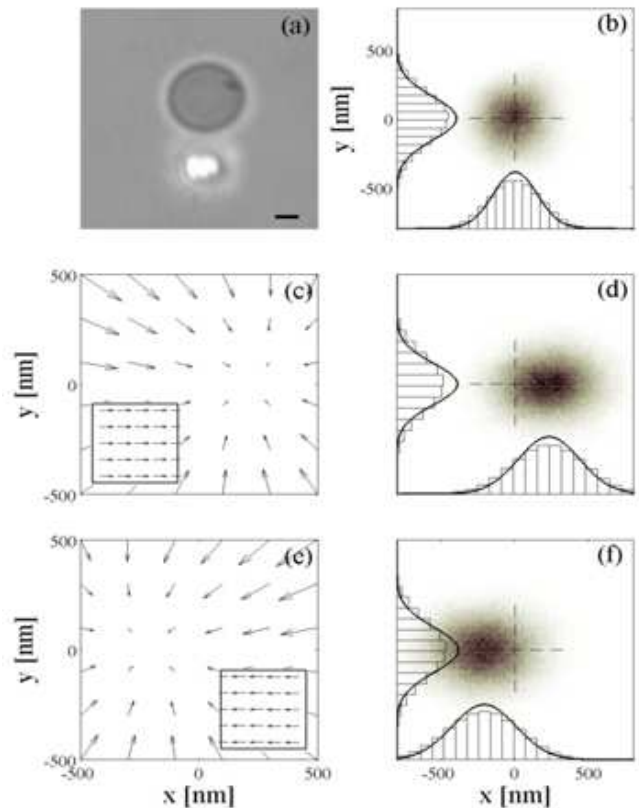


FIG. 1: (Color online) (a) Image of a trapped probe near a single spinning sphere. The bar is $1 \mu\text{m}$. (b) 2D Probability Density Function (PDF) when the spinning sphere is at rest. (c-f) Total force fields - insets: drag force field contribution - and 2D PDF when the sphere is spinning (c-d) counterclockwise and (e-f) clockwise. For each of the plots (b), (d), and (e) data acquired during 150 s with sampling rate 2000 Hz were analyzed.

flow velocity near a single spinning sphere [3, 6]

$$\mathbf{v} = \omega \mathbf{e}_z \times \mathbf{x} \frac{R^3}{\|\mathbf{x}\|^3}. \quad (1)$$

In each point near the rotating sphere the streamlines are perpendicular to the plane containing the z -axis (unit vector \mathbf{e}_z) and the coordinate vector \mathbf{x} .

In Fig. 1 the results for probing such a drag force field near a single spinning sphere are presented. The CVC sphere is put into rotation at $\omega \approx 38 \text{ rad/s}$. The induced drag force can be measured through the shift of the equilibrium position of the probe (Fig. 1(b), 1(d), and 1(f)) and after calibrating the stiffness of the probe trap ($k = 175 \pm 15 \text{ fN}/\mu\text{m}$). The corresponding force field can be reconstructed (Fig. 1(c) and 1(e)): the forces acting on the probe particle result $40 \pm 5 \text{ fN}$ (counterclockwise rotation) and $37 \pm 5 \text{ fN}$ (clockwise rotation). These results are in agreement with [5, 6].

In a system with n spinning spheres, the linearity of the quasi-Stokes equations [3] allows one to use the super-

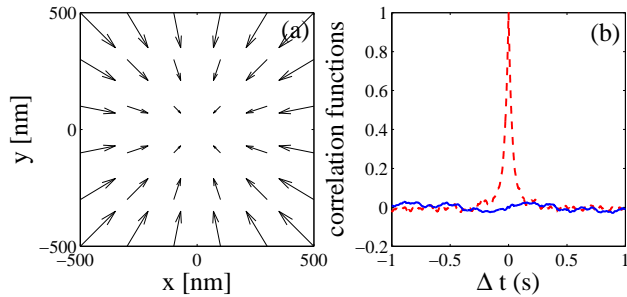


FIG. 2: (Color online) (a) Force field and (b) auto- (red dashed line) and cross-correlation (blue solid line) functions when only the optical force is acting on a $0.5 \mu m$ radius probe in absence of drag force field. For plot (b) data acquired during 150 s with sampling rate 2000 Hz were analyzed.

position of solutions (1) in order to obtain the total flow. Since the velocity in the equatorial plane is proportional to the reciprocal square of the distance from the sphere center, the flow velocity vanishes at a distance of a few sphere radii. Hence, in first approximation the hydrodynamic interaction between the spinning spheres located far enough from each other can be neglected. For $n = 2$ or $n = 4$ we assume the spheres to be symmetrically displaced at the same distance ρ with respect to the origin \mathbf{x}_0 (Fig. 3(a) and 4(a)), so that the origin is a singular point, i.e. $\mathbf{v}(\mathbf{x}_0) = 0$. The velocity field can be locally approximated as

$$\mathbf{v} = \omega R^3 \mathbf{J} \mathbf{x} = \omega R^3 \sum_{i=1}^n \mathbf{J}_i \mathbf{x}, \quad (2)$$

where \mathbf{J} is the Jacobian matrix of the total velocity field evaluated in the singular point and \mathbf{J}_i the Jacobian matrix of the velocity field generated by particle i evaluated in the same point. As expected, since the fluid is incompressible, $Tr(\mathbf{J})$ is always null. This means that only (unstable) saddles - with $n = 2$, $\det(\mathbf{J}) = -4/\rho < 0$ - or (stable) centra - with $n = 4$, $\det(\mathbf{J}) = 2/\rho > 0$ - can exist.

In Fig. 2 to 4 the experimental results for such cases are presented. We followed the data analysis procedure proposed in [18], to which we refer for the full details. The total force field acting on the probe is given by the sum of the drag force-field and the restoring force due to the harmonic trapping potential. The drag force field can be decomposed into a conservative and a rotational part, while the optical force field is purely conservative. The cross-correlation function (CCF) between the x and y position of the probe, calculated as $CCF(\Delta t) = \langle x(t)y(t+\Delta t) \rangle - \langle y(t)x(t+\Delta t) \rangle$, does not vanish only if the rotational part of the drag force field is not null. The rotational component of the drag force field can be obtained from the CCF [18, 19]. If the rotational component, and therefore the CCF, is null, the

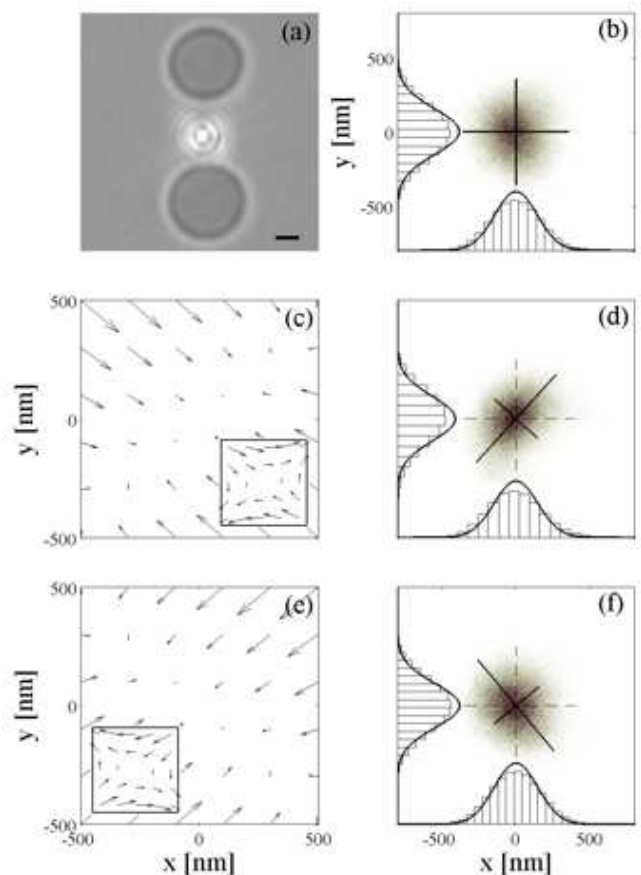


FIG. 3: (Color online) (a) Image of a trapped probe between a couple of spinning spheres. The bar is $1 \mu m$. (b) 2D Probability Density Function (PDF) when the spinning sphere is at rest. (c-f) Total force fields - insets: drag force field contribution - and 2D PDF when the sphere is spinning (c-d) counterclockwise and (e-f) clockwise. For each of the plots (b),(d), and (e) data acquired during 150 s with sampling rate 2000 Hz were analyzed.

total force field is purely conservative, and the conservative component of the drag force field can be calculated by subtracting the optical potential from the total potential. We underline that this can only be done if the total force field is conservative. Some results for an optically trapped probe in the absence of flow are presented in Fig. 2: the optical force-field is harmonic (Fig. 2(a)) and it is purely conservative, as it is shown by the fact that its CCF function is null (Fig. 2(b)).

In Fig. 3 the flow to be probed is generated putting into rotation ($\omega \approx 38 \text{ rad/s}$) two CVCs, symmetrically positioned with respect to the probe beads (Fig. 3(a)). The position of the probe is chosen so that there is no shift in the equilibrium position regardless of the rotation state of the spheres (Fig. 3(b), 3(d), and 3(f)). Since the experimental CCF is found to be null within the experimental error, we conclude that the rotational component of the drag force field must be negligible and

we can reconstruct its conservative part by subtracting the optical restoring force-field from the total force field (Fig. 3(c) and 3(e)). The optical trap produces a symmetric harmonic potential ($k = 185 \text{ fN}/\mu\text{m}$) (Fig. 3(b)). With spinning CVCs the PDF becomes ellipsoidal (Fig. 3(d) and 3(f)). For a clockwise rotation (Fig. 3(c-d)), the main axes of the ellipses are oriented at 40° , the stiffness is $k_{min} = 142 \text{ fN}/\mu\text{m}$ along the main axis and $k_{MAX} = 261 \text{ fN}/\mu\text{m}$ along the secondary axis. For a counterclockwise rotation (Fig. 3(e-f)), the main axes of the ellipses are oriented at 42° , the stiffness is $k_{min} = 165 \pm 20 \text{ fN}/\mu\text{m}$ along the main axis and $k_{MAX} = 211 \pm 20 \text{ fN}/\mu\text{m}$ along the secondary axis. The difference are due to the fact that the rotation rate was observed to be different in the two directions. The corresponding total force fields are represented in Fig. 3(c) and 3(e), while the drag force field contributions are depicted in the insets: they constitute indeed saddle points.

In Fig. 4 the characterization of a fluid flow near a singular point of the second kind, a centrum, is presented. This stable singular point was generated putting into rotation ($\omega \approx 38 \text{ rad/s}$) four birefringent spheres symmetrically distributed with respect to the probe (Fig. 4(a)) in an optical trap with stiffness $k = 78 \pm 5 \text{ fN}/\mu\text{m}$. We can observe that the PDF of the probe position do not depend on the rotation direction of the spinning spheres (Fig. 4(b)); however, in this case the CCF is not null (Fig. 4(d) and 4(f)), showing the presence of a rotational component of the drag force field. This component is such that it produces a torque on the probe bead, whose angular velocity is Ω , as $\gamma\Omega < x^2 + y^2 > = 5.7 \text{ fN}\mu\text{m}$ for the beads rotating clockwise (Fig. 4(c-d)) and $6.4 \text{ fN}\mu\text{m}$ for the case of the beads rotating counterclockwise (Fig. 4(e-f)). The resulting total and drag force fields are represented in Fig 4(c) and 4(e), while the drag force field contributions are depicted in the insets: they constitute, indeed, a centrum.

In conclusion, we have demonstrated the use of an optically trapped probe for the characterization of singular points in microscopic flows. This technique delivers an important contribution towards a better understanding and optimization of microfluidic flows in the presence of singular points, providing both a deeper understanding of their physics and an experimental approach to their characterization. Furthermore our approach allows one to determine the stability of these singular points, which can be relevant for applications.

The authors acknowledge useful discussions with N. Heckenberg, A. Bagnó, and M. Rubí. This research was carried out in the framework of ESF/PESC (Eurocores on Sons), through grant 02-PE-SONS-063-NOMSAN, and with the financial support of the Spanish Ministry of Education and Science. It was also partially supported by the Departament d'Universitats, Recerca i Societat de la Informació and the European Social Fund.

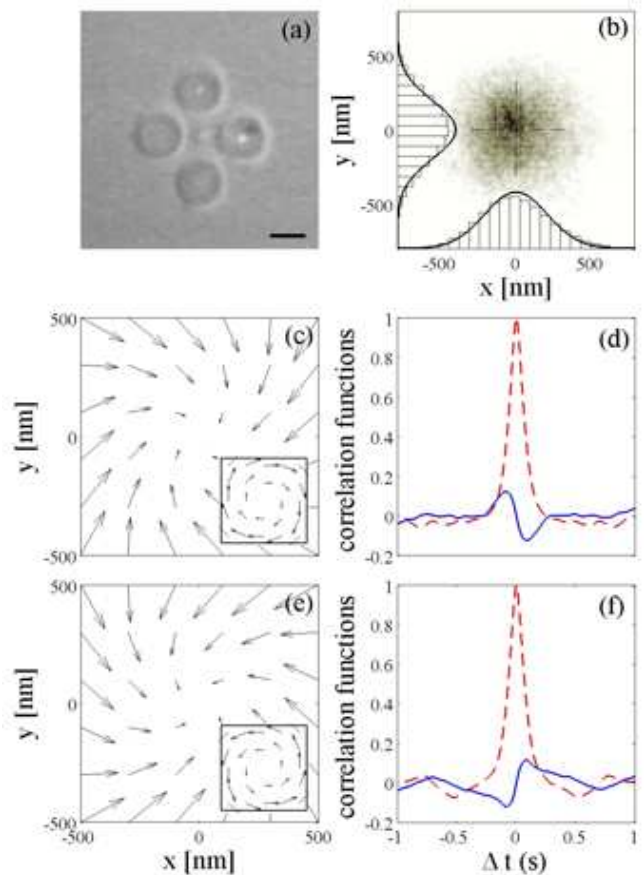


FIG. 4: (Color online) (a) Image of a trapped probe between four spinning spheres. The bar is $3 \mu\text{m}$. (b) 2D probability density function when the spinning sphere is at rest. (c-f) Total force fields - insets: drag force field contribution - and auto- (red dashed line) and cross-correlation (blue solid line) functions when the sphere is spinning (c-d) counterclockwise and (e-f) clockwise. For each of the plots (b),(d), and (e) ten datasets acquired during 15 s with sampling rate 2000 Hz were analyzed and averaged.

-
- [1] J. Knight, *Nature* **418**, 474 (2002).
 - [2] Y. Zhu and S. Granick, *Phys. Rev. Lett.* **87**, 096105 (2001).
 - [3] J. Happel and H. Brenner, *Low Reynolds Number Hydrodynamics* (Springer, New York, 1983).
 - [4] B. A. Nemet and M. Cronin-Golomb, *Opt. Lett.* **27**, 1357 (2002).
 - [5] A. I. Bishop, T. A. Nieminen, N. R. Heckenberg, and H. Rubinsztein-Dunlop, *Phys. Rev. Lett.* **92**, 198104 (2004).
 - [6] G. Knöner, S. Parkin, N. R. Heckenberg, and H. Rubinsztein-Dunlop, *Phys. Rev. E* **72**, 031507 (2005).
 - [7] G. Pesce, A. Sasso, and S. Fusco, *Rev. Sci. Instrumen.* **76**, 115105 (2006).
 - [8] R. Di Leonardo, J. Leach, H. Mushfique, J. M. Cooper, G. Ruocco, and M. J. Padgett, *Phys. Rev. Lett.* **96**, 134502 (2006).

- [9] K. C. Neuman and S. M. Block, *Rev. Sci. Instrumen.* **75**, 2787 (2004).
- [10] L. Ghislain and W. W. Webb, *Opt. Lett.* **18**, 1678 (1993).
- [11] J. H. E. Florin, A. Pralle and E. Stelzer, *J. Struct. Bio.* **119**, 202 (1997).
- [12] A. Rohrbach and E. Stelzer, *J. App. Phys.* **91** (2002).
- [13] K. Berg-Sørensen and H. Flyvbjerg, *Rev. Sci. Instrumen.* **75**, 594 (2004).
- [14] S. S. M.W.Hirsch and R. Devaney, *Differential Equations, Dynamical Systems, and an Introduction to Chaos* (San Diego, 2004).
- [15] A. D. Stroock, S. K. W. Dertinger, A. Ajdari, I. Mezić, H. A. Stone, and G. W. Whitesides, *Science* **295** (2002).
- [16] A. Belanger, *Vascular Anatomy and Physiology: An Introductory Text* (Davies publishing, Inc., 1990).
- [17] S. Q. Liu, L. Zhong, and J. Goldman, *Trans. ASME* **124**, 30 (2002).
- [18] G. Volpe, G. Volpe, and D. Petrov (2007).
- [19] G. Volpe and D. Petrov, *Phys. Rev. Lett.* **97**, 210603 (2006).